Int. J. Heat Mass Transfer. Vol. 33, No. 10, pp. 2145–2159, 1990
Printed in Great Britain

0017–9310/90 $3.00 + 0.00

Buoyancy induced instability of laminar flows in vertical annuli—I. Flow visualization and heat transfer experiments

MOHAMED S. EL-GENK and DASARI V. RAO
Department of Chemical and Nuclear Engineering, The University of New Mexico, Albuquerque, NM 87131, U.S.A.

(*Received* 11 *April* 1989 *and in final form* 11 *December* 1989)

Abstract—Experiments encompassing both flow visualization and heat transfer measurements ($125 < Re_{in} < 1700$ and $2.5 \times 10^5 < Gr_q < 5 \times 10^7$) are performed to investigate buoyancy induced instability of developing laminar upflow and downflow of water in a vertical annulus having a diameter ratio of 2.0. The inner wall of the annulus is uniformly heated and the outer wall is insulated. Incipient flow instability is detected from the video images of the dyed flow field, the simultaneous decrease in the temperature difference between the heated wall and the water bulk from its laminar value and the fluctuations in the coolant temperature. The measured values of x_{fr}, based on the video images of the dyed flow fields, are correlated for both buoyancy assisted and opposed flows as functions of local Grashof number, Gr_q, and local Reynolds number, Re. The Nusselt numbers for buoyancy induced turbulent flows, occurring downstream of the location of incipient instability, are as much as three times higher than those for stable laminar flows at the same inlet Reynolds number, but at lower Gr_q. The heat transfer data for buoyancy induced turbulent flows are correlated as:

$$Nu = 0.088\, Ra_q^{0.33}\, Re_{in}^{-0.12}, \quad \text{for upflow}$$

$$Nu = 0.21\, Ra_q^{0.29}\, Re_{in}^{-0.12}, \quad \text{for downflow.}$$

INTRODUCTION

IN LAMINAR flows of water in vertical annuli hydrodynamic instability arises when the induced variations in the density and viscosity with temperature distort the axial velocity field, causing a disturbance which grows as it is convected downstream [1]. However, the degree to which the axial velocity profile in the annular gap is distorted depends on the flow direction and the relative magnitudes of the buoyant and inertial forces. At the onset of flow instability, flow stagnation may occur near the outer adiabatic wall or near the inner heated wall, for buoyancy assisted and opposed flow, respectively. Beyond this point, referred to as 'location of incipient flow instability' or 'location of flow transition', x_{fr}, the disturbances grow giving rise to turbulent flow. For boundary layer flows the transition criteria have been displayed by the simultaneous presence of significant temperature fluctuations and a decrease in the temperature difference across the boundary layer from its laminar value for isoflux condition [1]; these criteria were verified in this research.

Numerous studies investigating the transition of natural and forced laminar flows of water in vertical annuli and tubes have been performed [2–7]. However, no correlations for predicting the location of incipient flow instability, x_{fr}, were reported. Also, heat transfer data for buoyancy induced turbulent flow, downstream of the location of flow transition, is minimal and heat transfer correlations are nonexistent [2, 3]. Most experimental and theoretical investigations have focused only on studying the conditions leading to the onset of flow instability and on relating these conditions to the magnitude of the induced distortion in the velocity profile [2–10].

Although the results of experiments investigating flow instabilities in other geometries (such as vertical tubes, open channels and between parallel plates) are not applicable to annular geometry, they are briefly reviewed here because the phenomena and conditions marking the onset of flow instability are similar. Hanratty *et al.* [4], Sheele and Hanratty [5], Hallman [6], and Sheele *et al.* [7] have experimentally studied the instabilities of combined natural and forced laminar flows of water in uniformly heated vertical tubes. Sheele and Hanratty [5] varied the length of the test section from 152 to 762 tube diameters. They determined the ratios of heat flux to mass flow rate (Gr_q/Re) for inducing flow instabilities at the exit of the test section as a function of inlet Reynolds number. To visualize the flow field and detect the onset of flow instability, Hanratty *et al.* [4], Sheele and Hanratty [5], and Sheele *et al.* [7] used the dye-injection technique. Observation of flow fields by Sheele and Hanratty [5], and Sheele *et al.* [7] revealed that in buoyancy assisted flow the transition to turbulent flow occurred through a gradual growth of small disturbances. However, for buoyancy opposed flow, this transition occurred suddenly, inducing flow mixing that typifies turbulent

NOMENCLATURE

A_c	cross sectional flow area [m^2]
C_p	specific heat [$kJ\,kg^{-1}$]
D	diameter [m]
D_e	equivalent diameter, $(D_o - D_i)$ [m]
g	acceleration due to gravity, 9.81 $m\,s^{-2}$
Gr_q	Grashof number, $g\beta D_e^4 q/\nu^2 k$
k	thermal conductivity [$W\,m^{-1}\,K^{-1}$]
L	length of the heated section [m]
$\dot{m}$	mass flow through the annulus [$kg\,s^{-1}$]
Nu	Nusselt number, $qD_e/k(T_w - T_b)$
P	total power to the heater [W]
Pr	Prandtl number, $\mu C_p/k$
q	surface heat flux, $P/\pi D_i L$ [$W\,m^{-2}$]
Ra_q	Rayleigh number, $Gr_q \cdot Pr$
Re	Reynolds number, $\dot{m}D_e/A_c\mu$
T	temperature [K]
ΔT	temperature drop across the boundary layer, $T_w - T_b$
x	axial distance measured from the entrance of the heated section in the direction of the flow [m]
X	dimensionless axial distance, x/D_e
ΔX	dimensionless distance measured from the location of incipient flow instability in the direction of the flow.

Greek symbols

β	coefficient of volumetric expansion [K^{-1}]
ε	annulus ratio, D_o/D_i
μ	dynamic viscosity of water [$kg\,m^{-2}s^{-1}$]
ν	kinematic viscosity [$m^2\,s^{-1}$]
ρ	density of water [$kg\,m^{-3}$].

Subscripts

b	water bulk temperature
fr	location of incipient instability
i	inner heated stainless steel tube
in	inlet of the test section
o	outer wall of the annulus
tr	incipient flow instability at the exit of the heated section
w	heated wall.

flow. As discussed later, a similar behavior was observed in the present experiments for water flows in a vertical annulus with a uniform wall heat flux.

Rosen and Hanratty [3] developed a simplified model, based on an approximate solution of the boundary layer equations, to predict the onset of flow instability in vertical tubes with an isothermal wall. The location of incipient flow instability was interpreted as that at which both the axial velocity and its radial gradient vanish at the center of the tube. They compared the model predictions with the experimental data of Sheele *et al.* [7]. At low Gr/Re values ($Gr_q/Re < 500$) the flow instability occurred far downstream ($(x_{fr}/\pi D\ Re\ Pr) > 20$), which is indicative of fully developed flow, and the agreement between the model predictions and the experimental data was good. However, when $Gr/Re > 500$ flow transition occurred very close to the start of the heated section, which is a case of developing flow, the model underpredicted the values of x_{fr} by as much as 65%. This discrepancy was partially attributed to the invalidity of the boundary layer solution, which excludes the radial momentum transfer, to describe the developing flow [3]. In a companion paper by the authors the effect of radial momentum transfer on x_{fr} is quantified for vertical annuli with isoflux heating and found to be important for developing flows [11].

In a separate investigation of combined laminar flow in vertical tubes with uniform wall heat flux, Hallman [6] measured x_{fr} as a function of the inlet Reynolds number and the surface heat flux. Instead of the dye-injection technique, Hallman [6] used wall thermocouples to detect the location of incipient flow instability. However, it was difficult to accurately determine the values of x_{fr} because the wall temperature thermocouples were placed about 5 cm apart and the wall temperature fluctuations were damped by the heat capacity of the tube. Based on his own data, Hallman proposed an empirical criterion, relating Ra, evaluated at the local film temperature, to the local Graetz number ($Re\ Pr\ D/x_{fr}$), for predicting the transition to turbulent flow. This criterion was later used by Metais and Eckert [12] to demarcate laminar and turbulent flows in their flow regime map. The validity of Hallman's criterion has never been verified for developing flow at high heat fluxes nor for other geometries.

Mullin and Gerhard [8] studied the heat transfer in downward flow of water in vertical tubes with uniform wall temperature at low Graetz numbers ($Gz < 400$). They found that Nusselt numbers for heating were higher than might be expected for stable laminar downflow, and were slightly higher than or about the same as those for upflow. They attributed this enhancement in the heat transfer rate to the occurrence of flow instabilities similar to those observed by Sheele *et al.* [7]. Other experiments investigating the effect of buoyant forces on heat transfer in laminar downflow of air between two vertical parallel plates have shown that raising the heat flux destabilizes the boundary layer adjacent to the heated surface, thus increasing the heat transfer coefficient [13, 14]. However, no heat transfer correlations were proposed for predicting the heat transfer rates.

It is evident that additional experiments and modeling of developing laminar flow in vertical annuli are needed to accurately predict the location of incipient flow instability as well as to measure and correlate the

heat transfer data in the downstream turbulent flow region. To characterize the onset of flow transition and quantify its effect on heat transfer, this research performed flow visualization and heat transfer experiments for both buoyancy assisted and opposed flows. The experiments used both the dye-injection and wall and coolant temperature traces techniques to determine the location of incipient flow transition in a vertical annulus having a uniformly heated inner wall and an adiabatic outer wall. In addition, the measured Nusselt numbers for buoyancy induced turbulent flows were correlated and compared with those reported previously for forced and combined laminar flows at the same Re_{in}, but at lower Gr_q values [15].

Description of the test section

The present annulus of $\varepsilon = 2.0$ consists of a uniformly heated 316 stainless steel tube, 12.7 mm o.d., 90 cm long and 0.6 mm thick, and an insulated plexiglas tube of 25.4 mm i.d. The stainless steel tube was silver brazed at both ends to brass tubes; each was 22 cm long and 12.7 mm in diameter. Each brass tube was then screwed into a copper connector, 40 mm o.d. and 22 cm long for connecting the test section to a 200 kW d.c. power supply. Each copper connector had a central hole, 15 mm in diameter, all along its length to allow access for measuring the temperature at the inner surface of the heated tube. Gold washers were placed between the brass tubes and the copper connectors to ensure good electrical contact. The heat generated in the brass tubes and the copper connectors was very small (< 1%) compared to that generated in the stainless steel tube. The test section, vertically centered inside the plexiglas tube, was mounted between two aluminum headers; each was 20 cm high and 20 cm i.d. These headers were included in the design of the test section to: (a) provide mixing of the water at both the entrance and the exit of the test section, (b) provide a flat axial velocity profile at the entrance to the annulus, and (c) neutralize any pumping induced instabilities, if present. The flow was then allowed to hydrodynamically develop while flowing through the unheated part of the annulus that precedes the heated stainless steel tube. Figure 1 shows the longitudinal cross section of the test section.

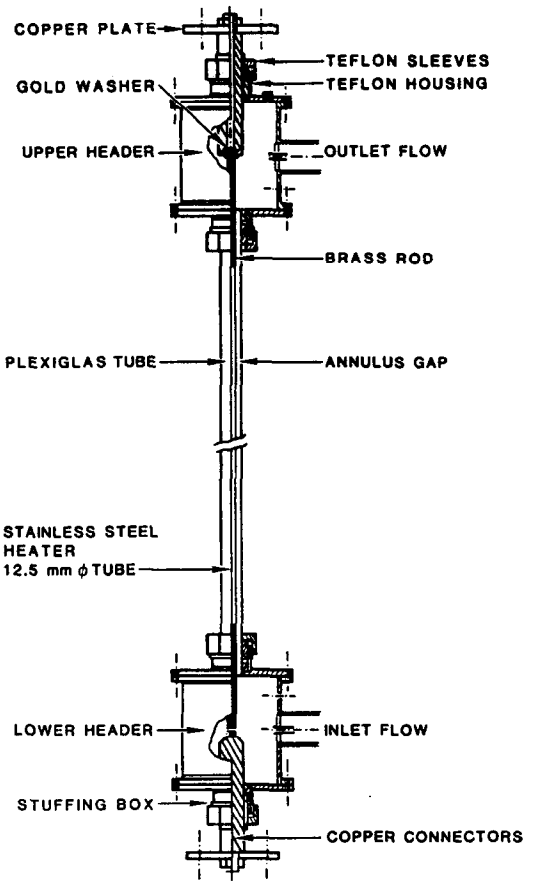

FIG. 1. Cross-sectional view of the test section employed in the experiment.

Experimental measurements

Because the heat generated in the stainless steel tube is directly related to its electric resistivity, it was not possible to measure the surface temperatures using spot welded thermocouples. Such spot welding would have altered the thickness of the tube and, consequently, would have reduced the local heat generation of the weld. Additionally, placing the thermocouple leads along the outer surface of the tube would not only have disturbed the flow fields but would have changed the heat transfer due to the fin effect. To avoid such uncertainties, a special probe was designed for measuring the temperature of the inner surface of the heated tube [15]. The surface temperatures of the heated wall were obtained from the temperatures measured at the inner surface of the heated tube after correcting for the temperature drop (of the order of 0.5 K) across the wall (thickness 0.6 mm).

The coolant temperatures were monitored near the outer adiabatic wall at seven axial locations, 20, 30, 40, 50, 60, 70, and 80 cm from the bottom of the heated section. Although the surface temperatures of the heated tube were only measured at five locations at a time, the temperature probe was adjusted inside the tube so that the wall surface temperatures could be measured at the same seven axial locations as the coolant temperatures. In this paper the *coolant temperature* refers to the water temperature near the outer wall of the annulus (≈ 1 mm from the inner surface of the wall) which differs from the bulk temperature obtained from the heat balance. The bulk temperature was used to evaluate the local values of Nusselt numbers and other dimensionless quantities. All the temperature measurements, conducted using ungrounded OMEGA brand K-type (chromel–alumel) stainless steel thermocouples, were within $\pm 0.3\%$ of the exact values over the entire temperature range in the experiments (288–358 K).

During the upflow experiments the water rates

through the test section were directly measured using a Dwyer rotometer (0.2–2.0 GPM) and Signet turbine meter (2.0–20.0 GPM). In the downflow experiments, however, the water flow rate was measured by performing a heat balance using the recorded rise in the water temperature across the heated section. To confirm the results of the heat balance, the flow rates in the downflow experiments were also measured using the weight/time method. The difference between these flow rates and those determined from the heat balance were within $\pm 5\%$. The energy dissipation in the stainless steel tube was determined from the voltage and current readings of the power supply after subtracting the power losses in the electric cables, brass tubes, and electric connectors (7.3%). The uncertainties in the electric power readings were less than 2%. More details on the uncertainties in the heat transfer data and measurements are available elsewhere [15].

Experimental conduct

In each experiment, the mass flow rate through the annulus was kept constant while the electric power to the heated section was incremently increased until flow instability occurred near the exit of the heated section. At each increment, the electric power to the test section was kept constant and a dye solution was injected into the flow stream. The dyed images of the flow field were recorded on a video tape and viewed on a video monitor. Because the injection of the dye solution into the annular gap amounts to an incremental increase in the mass flow rate, sometimes up to 2%, temperature measurements were recorded only after the dye solution was completely cleared from the annular gap. In the experiments, the surface temperatures of the heated section were kept below 358 K to avoid disturbing the boundary layer at the heated wall by the release of dissolved gases. This temperature is slightly lower than the water boiling temperature (367.4 K) in Albuquerque, New Mexico.

The Reynolds numbers were varied from 330 to 1100 for upflow and from 100 to 1133 for downflow while the heat flux was increased in small increments up to 7.8×10^4 and 7.23×10^4 W m^{-2} for upflow and downflow, respectively. The experimental conditions were established so that the ratio of the water viscosity at the heated wall to that at the inner surface of the outer wall was between 6.5 and 4.0 for upflow and between 7.0 and 4.0 for downflow while the inlet temperatures varied between 288 and 308 K.

Flow visualization

The flow visualization experiments employed two techniques for detecting the onset of flow instability: (a) dye solution injection, and (b) wall and coolant temperature traces. In the first method, the flow field was characterized by injecting a thin filament of dye solution into the flow stream. For this purpose the test section was equipped with two fine syringes placed 8 cm above and below the heated section. While the syringe needle was bent in the direction of the flow to avoid disturbing the flow field, the tip of the syringe needle was perpendicular to the flow direction to minimize the jet effect of the injected dye solution. In this configuration the dye solution lost its imparted energy while traveling in the radial direction, and thereafter traveled with water in the annular gap. The density of the dye solution employed in the present experiments was equal to that of water. The images of the dye flow fields were documented by still photographs (a representative photograph is presented later in the paper) and on a video tape. The video images, captured using a Panasonic video camera with magnification of approximately 250% were used to determine the location of the onset of flow instability in both the upflow and downflow experiments.

In the second method, the onset of flow instability was detected by monitoring the recorded traces of the surface and the coolant temperatures' thermocouples. When flow instabilities ensued, the heater's surface temperatures downstream and, also occasionally upstream of that location, underwent random oscillations. However, the random oscillations of the coolant temperatures occurred only downstream of the location of incipient flow instability. The location of incipient instability was also detected from the decrease in the measured temperature difference between the heated wall and the water bulk below that of stable laminar flow at the same inlet Reynolds number. Subsequently, the coolant thermocouple traces were used to determine the approximate location of the onset of flow instability. However, since the coolant thermocouples were placed 10 cm apart, more accurate determination of the location of the onset of flow instability was obtained from the video images of the flow field. The uncertainties in determining the location of incipient flow instability from the video images were within ± 10 and 20% for buoyancy assisted and opposed flows, respectively.

RESULTS AND DISCUSSIONS

At a given inlet Reynolds number and for Gr_q values less than that required to initiate flow instability at the exit of the heated section, $(Gr_q)_{tr}$, the flow was stable along the entire length of the annular test section [15]. The stability of the flow at these low heating rates was confirmed by injecting a thin filament of dye solution into the annular gap and observing the flow field. The dye filament was continuous over the entire length of the test section. As the heating rate increased and Gr_q approached $(Gr_q)_{tr}$, the otherwise stable dye filament started fluctuating at the exit of the heated section indicating the onset of flow instability at that location. This observation was true for both buoyancy assisted and opposed flows. Increasing Gr_q beyond $(Gr_q)_{tr}$ moved the location of incipient closer to the entrance of the heated section. A similar observation was reported by previous investigators [4–7]. They only measured $(Gr_q)_{tr}$ as a function of Re_{in}. However,

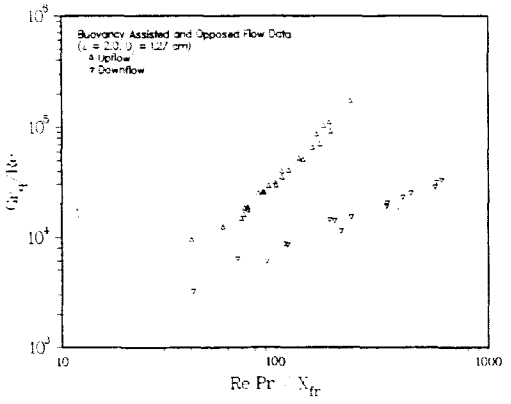

FIG. 2. Experimental data of X_{fr} for buoyancy assisted and opposed laminar flows in a vertical annulus having a diameter ratio of 2.

in the present study x_{fr} was measured as a function of Gr_q and both local Re and Re_{in}. Figure 2 presents the measured values of x_{fr} as (Gr_q/Re) vs $(Re\ Pr\ D_e/x_{fr})$ for both buoyancy assisted and opposed flows. As evident from this figure at the same $(Re\ Pr\ D_e/x_{fr})$ the value of Gr_q required to initiate instability for buoyancy assisted flow is larger than that for buoyancy opposed flow. Results in Fig. 2 also show that for a given Re and Pr values, increasing Gr_q/Re moves x_{fr} closer to the entrance of the heated section.

In ref. [11] the experimental measurements of x_{fr} were compared with the predictions of a numerical model based on the elliptic Navier–Stokes equations. In the model the location of incipient instability was defined as that where the radial gradient of the axial velocity (near the inner surface of the outer adiabatic wall or near the inner heated wall for buoyancy assisted and opposed flows, respectively) becomes equal to zero. The model predictions of x_{fr} were in reasonable agreement with the data (see Figs. 2 and 3 in ref. [11]).

Based on the model and experimental results the following criteria for incipient flow instability were proposed for buoyancy assisted and opposed flows in vertical annuli [11]

$$[(Gr_q/Re)-(Gr_q/Re)_{cr}] = A(Re\,Pr/X_{fr})^b(\varepsilon+1) \quad (1)$$

where $(Gr_q/Re)_{cr} = 3850$, $A = 0.18$ and $b = 2.32$, for upflow, and $(Gr_q/Re)_{cr} = 1500$, $A = 15.15$ and $b = 0.9$, for downflow. These criteria were in good agreement with the experimental data for both buoyancy assisted and opposed flows (see Fig. 11 of ref. [11]).

Flow field characterization

In addition to determining the values of x_{fr}, the flow visualization experiments also provided crucial information for characterizing the flow fields both upstream and downstream of the location of incipient flow instability. The following sections present and discuss the observed flow field characteristics for buoyancy assisted and opposed flows.

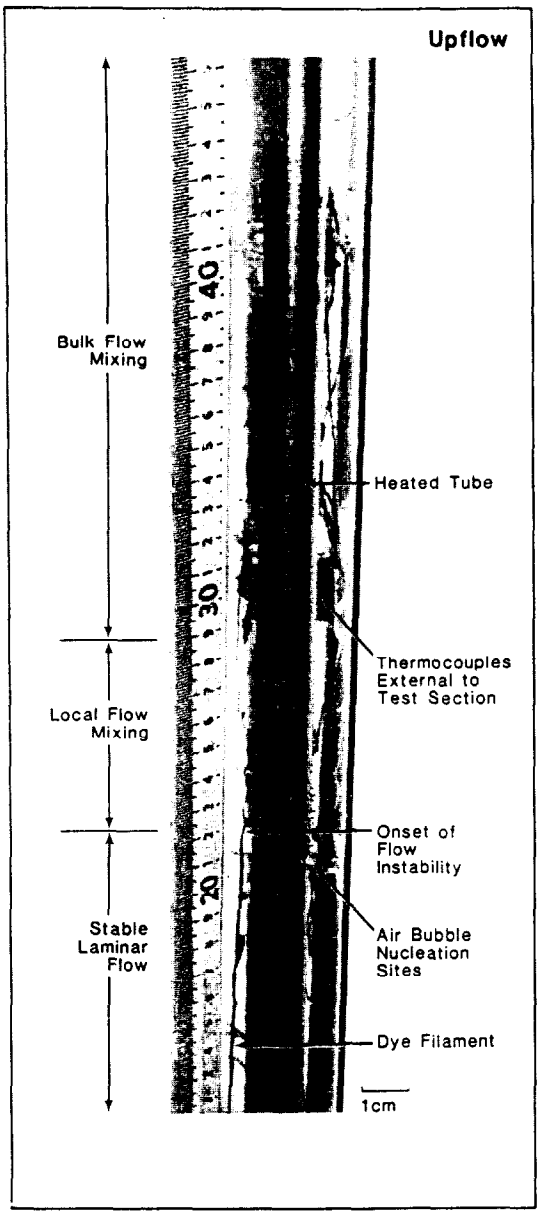

FIG. 3. A pictorial view of the transition of laminar upflow to buoyancy induced turbulent flow.

Buoyancy assisted flow visualization results

Figures 3 and 4 present photographic images of the flow fields for buoyancy assisted flow at Gr_q of 4.76×10^6 and Re_{in} of 500. As Fig. 3 shows, the dye filament was stable up to 22 cm from the entrance; then, it started oscillating immediately downstream of this location. The flow became increasingly unstable in the next 7 cm but the observed mixing was moderate. In the region that extended from the 29 cm mark to the top of the heated section, where the flow became turbulent, the dye solution was thoroughly mixed with water.

Figure 5(a), an artist's conception of the observed flow fields, indicates that the flow field in a buoyancy assisted flow can be divided into three successive regions.

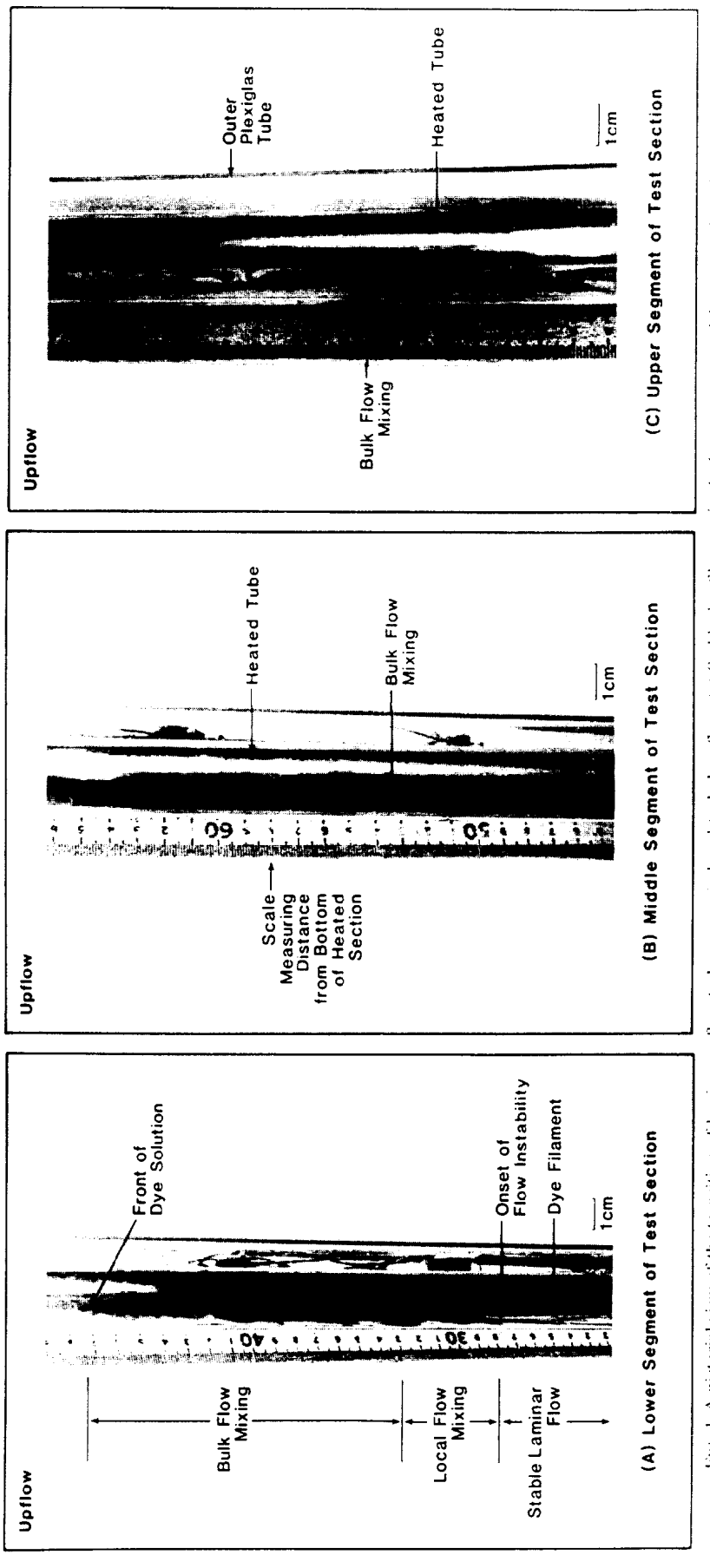

FIG. 4. A pictorial view of the transition of laminar upflow to buoyancy induced turbulent flow. (a) Stable dye filament in the lower segment of the test section. (b) Middle segment of the test section. (c) Upper segment of the test section.

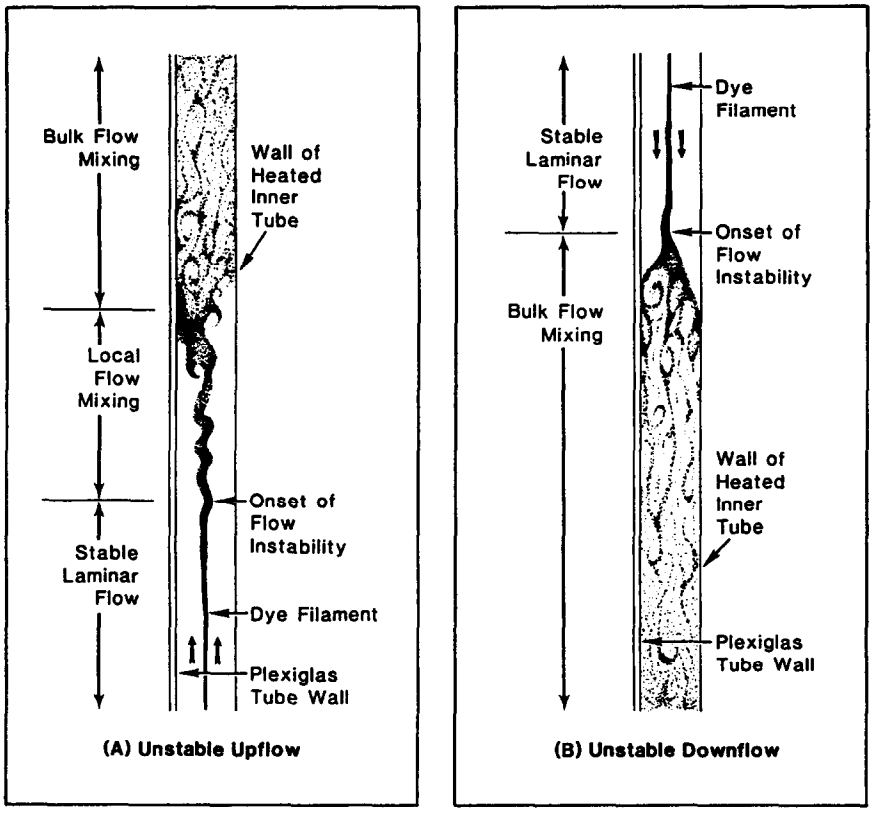

FIG. 5. Artist's conception of the transition of laminar upflow and downflow to buoyancy induced turbulent flow in vertical annuli.

(a) *A stable laminar flow region* exists at the entrance to the heated section where the dye filament is stable and continuous.

(b) *A local flow mixing (transition) region* is a short region downstream of the stable laminar flow region. This region is highlighted by formation of vortices near the outer wall. The flow mixing in this region is moderate and, as will be shown later, its influence on the heat transfer is moderate.

(c) *A turbulent flow region* succeeds the local flow mixing region and is characterized by extensive turbulent mixing. Figures 3 and 4 illustrate the prevailing turbulence in this region.

Buoyancy opposed flow visualization results

Figure 5(b) is an artistic conception illustrating the observed flow fields in buoyancy opposed flow experiments. Unlike buoyancy assisted flow, the flow field for buoyancy opposed flow consists only of two successive regions.

(a) *A stable laminar flow region* exists at the entrance of the heated section where the dye filament is stable and continuous.

(b) *A turbulent flow region* exists immediately downstream of the stable laminar flow region. In this region turbulent mixing of the dye solution with water occurs. Unlike buoyancy assisted flow, the transition from stable laminar to turbulent mixing conditions in buoyancy opposed flow was abrupt and a local flow mixing region was not observed, which is in agreement with the reported results for tube flows [5, 7].

Temperature traces technique for detecting the onset of flow instability

The temperature traces method has been used to detect the onset of flow instability in both buoyancy assisted and opposed flows [6]. While the flow visualization techniques provide information regarding the hydrodynamic transition, the temperature traces provide information pertaining to the thermal boundary layer transition. The coolant and wall thermocouples were monitored using a HP3947A data logger. Because the data logger was monitoring 18 channels simultaneously (a total of 15 thermocouples, one flowmeter, and one each of current and voltmeters), the temperature of each thermocouple was recorded only five times every second. Because the recording time of the temperature traces (200 ms) is significantly larger than the response time of the thermocouples (10 μs), it was not possible to quantify the frequency of the temperature fluctuations accurately. Despite this shortcoming the thermocouple traces provided

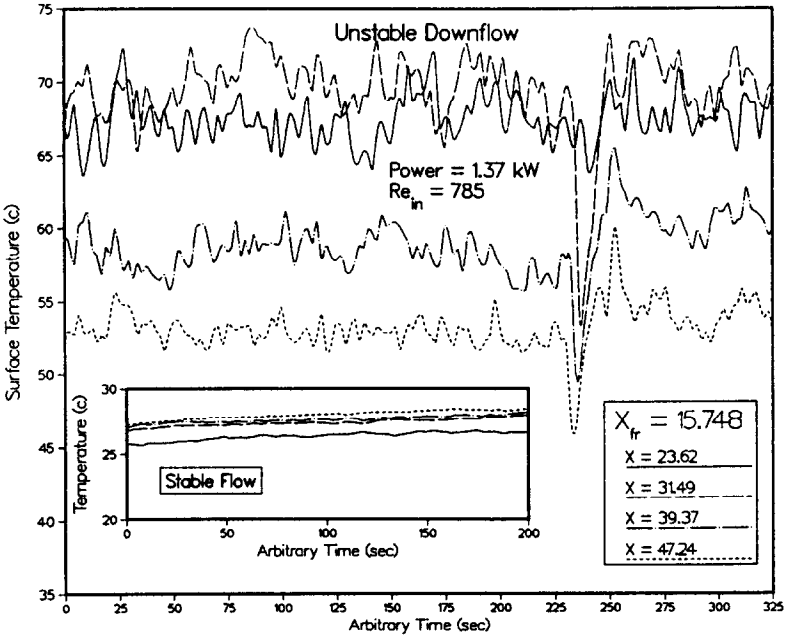

FIG. 6. Typical wall temperature traces marking the transition of laminar downflow to buoyancy induced turbulent flow.

very valuable information regarding the detection of flow instability. In Figs. 6–11, the values of X_{fr} were determined from the video images of the dyed flow fields.

Figure 6 presents typical wall surface temperature traces for the buoyancy opposed flow downstream from the location of incipient flow instability ($X_{fr} \approx 15.748$). As this figure shows, the transition to turbulence has introduced random oscillations in the wall temperatures. Although, most of the times wall temperature oscillations were observed only downstream of x_{fr}, occasionally thermocouple readings a few centimeters upstream were also seen to fluctuate.

The coolant temperature traces measured 1–2 mm from the outer adiabatic wall are presented in Fig. 7. As this figure shows, the fluctuations in the coolant temperature occurred only downstream of x_{fr}; the temperature traces upstream of x_{fr} were very similar to those for stable laminar flow. In Fig. 7 note that the axial location at which $\Delta X = 0$, marks the onset of flow instability and that the negative and positive values of ΔX indicate upstream and downstream locations, respectively. As Fig. 7 demonstrates, the amplitude of the temperature oscillations decreased with the distance downstream of the location of incipient flow instability. These results suggest that the traces of the coolant temperature, if detected very close to each other without disturbing the flow field, could be used to determine the location of incipient flow instability, in lieu of visual observation. This finding is very important, since in most practical applications visual observation of the flow field is not possible.

It should be noted that while the video images of the flow field allow for measuring the values of x_{fr} due to hydrodynamic transition of the flow, the thermocouples detect the thermal transition that follows. However, because the thermocouples were placed 10 cm apart, the measurement of the location of thermal transition in these experiments is not exact and should be treated as approximate. Due to this drawback the correlations for x_{fr} reported in this paper as well as the companion paper pertain only to the hydrodynamic transition.

Figure 8 presents measured traces of the heater's surface temperatures for unstable upflow. As this figure demonstrates, the oscillations of the heater's surface temperatures are less frequent and much less intense than those for buoyancy opposed flow (see Fig. 6). Figure 9 plots the coolant temperature traces measured for upflow at various axial locations, both upstream and downstream of the location of incipient flow instability. Similar to buoyancy opposed flow, the coolant temperatures for buoyancy assisted flow only oscillated downstream of the location of incipient flow instability. A comparison of Fig. 7 and Fig. 9 indicates the differences in the frequency and intensity of oscillations of the coolant temperatures for both upflow and downflow.

The occurrence as well as the location of incipient flow instability for both buoyancy assisted and opposed turbulent flows were also detected by comparing the temperature differences between the heated wall and the water bulk temperature, ΔT, with those for stable laminar flows at the same Re_{in}. As pointed out earlier, beyond the location of transition in natural convection over vertical surfaces, a decrease of the temperature difference across the boundary layer

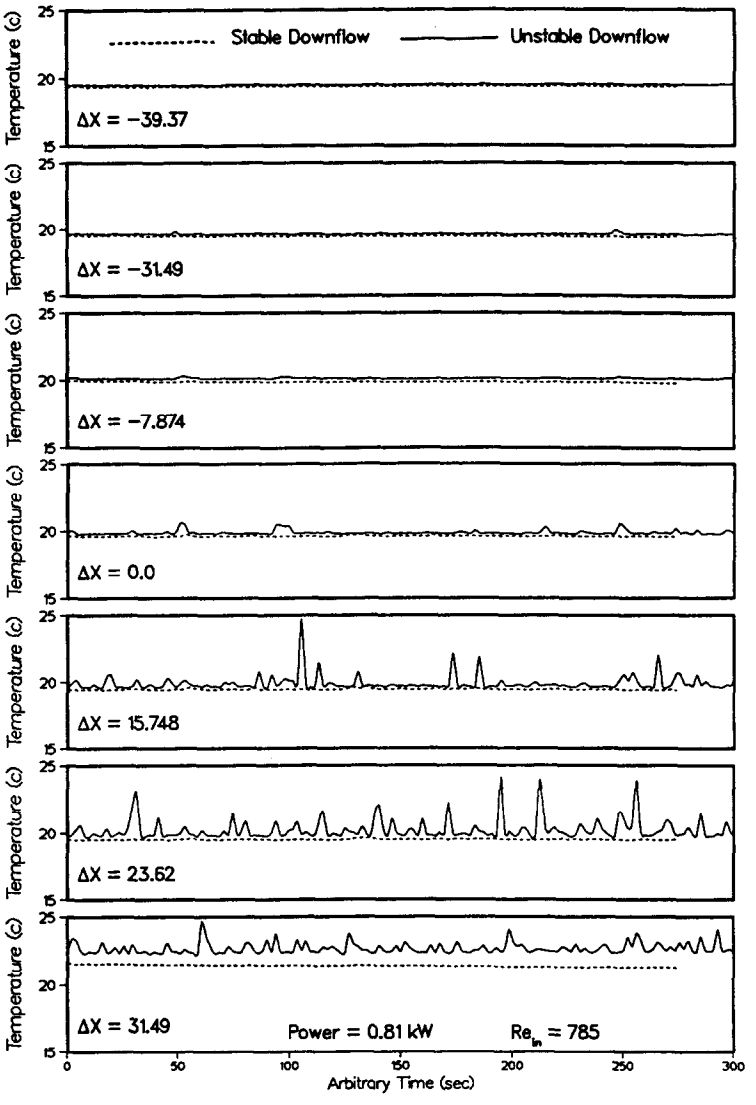

FIG. 7. Typical bulk temperature traces marking the transition of laminar downflow to buoyancy induced turbulent flow.

below its laminar value is reported [1]. Measurement of ΔT values in the present study confirmed this observation (see Figs. 10 and 11). In Figs. 10 and 11 the measured values of ΔT are plotted as functions of axial distance from the entrance of the heated section for both downflow and upflow, respectively. These values are also compared with those predicted for stable laminar flows of water using the heat transfer correlations developed in a previous study [15] to illustrate the effect of flow instability on ΔT. These results, in addition to those presented in Figs. 6–9, suggest that the wall and water temperature traces could be used to detect flow transition in lieu of the flow field visualization in applications where the latter is not possible.

In order to examine the effect of flow instability on heat transfer, data were collected for both buoyancy assisted and opposed flows and compared with those obtained previously for stable flows using the same test section [15]. The results of this comparison are presented and discussed in the following section.

Effect of flow instability on heat transfer

In order to determine the effects of flow instabilities on heat transfer for both buoyancy assisted and opposed laminar flows, a total of more than 300 heat transfer data points were collected from the experiments in which the heat flux represented by Gr_q, and the water flow rate, represented by Re_{in}, were varied independently. To average the effect of the random fluctuations in the local heater's surface temperature, chronological averages of the temperatures collected at a single location over a recording period of 120 s were used as the corresponding average local wall temperature. The water bulk temperature at required locations was determined from the heat balance in the

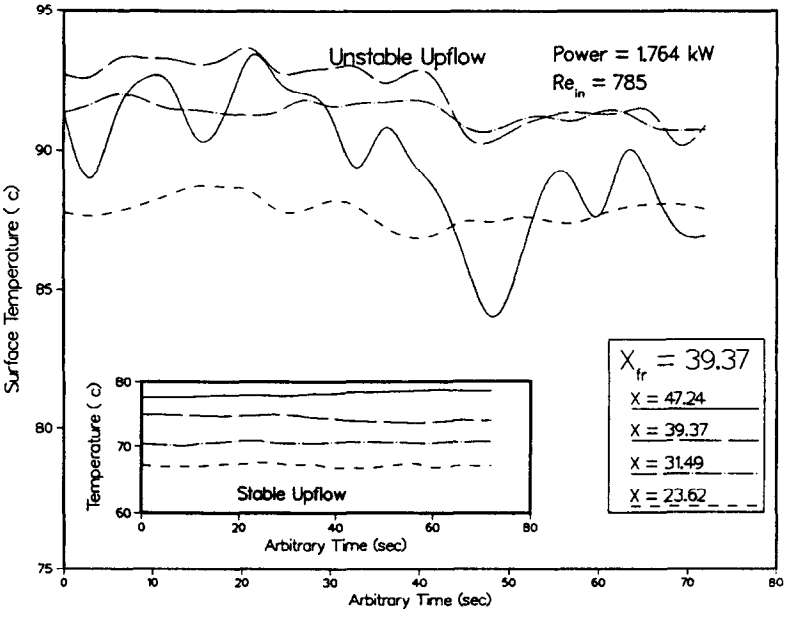

FIG. 8. Typical wall temperature traces marking the transition of laminar upflow to buoyancy induced turbulent flow.

test section, then used to calculate the values of the local Nusselt number and Grashof number.

To establish the sensitivity of the developed correlation to the temperature used to assess the thermal properties of the water, the average Nusselt numbers in the test section were correlated as functions of Gr_q and Re. These were evaluated at the inlet temperature, exit temperature, and at the average of the inlet and outlet temperatures. The correlation based on the inlet temperature, which varied between 288 and 308 K, provided the best agreement with the experimental results. The results indicate that at low Gr_q, stable laminar flow prevailed and that Nu values increased with Gr_q for buoyancy assisted flow, but decreased with Gr_q for buoyancy opposed flow. For Gr_q values exceeding those corresponding to the onset of flow instability, Nu for both buoyancy assisted and opposed flows increased rapidly as Gr_q increased. The results presented in Figs. 12 and 13 establish that Nu values for unstable flows were as much as three times higher than those for stable laminar flows at the same inlet Reynolds number but at lower Gr_q. This remarkable increase in the heat transfer rate for unstable flows is a direct consequence of the turbulent mixing characteristic of these flows.

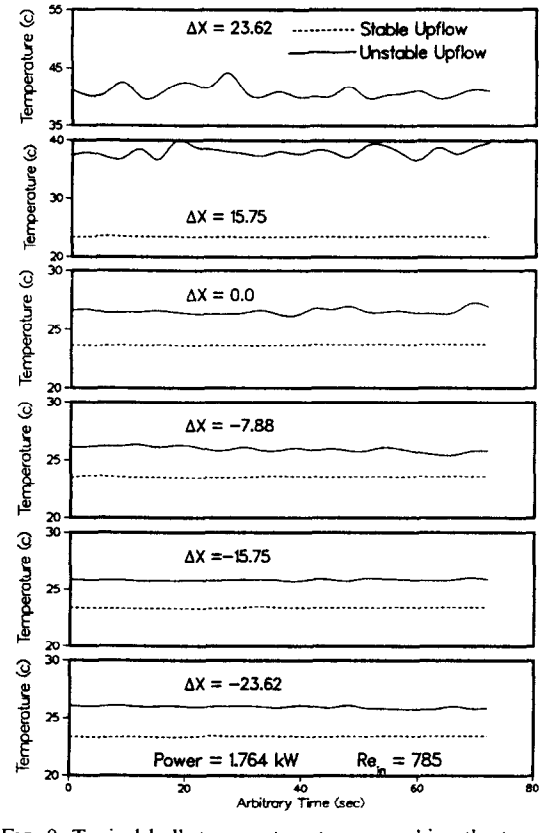

FIG. 9. Typical bulk temperature traces marking the transition of laminar upflow to buoyancy induced turbulent flow.

The results also demonstrate the difference in behavior between buoyancy assisted and buoyancy opposed flows. Figure 12 indicates that the transition in downflow from stable to unstable flow happened suddenly; this behavior was confirmed by the recorded video images of the flow field (see Fig. 5(b)). In buoyancy assisted flow, however, the transition from stable to unstable flow happened gradually, and an intermediate transition region occurs between the stable and the turbulent flow regions. In this intermediate region, the values of Gr_q are slightly higher than $(Gr_q)_{tr}$, and Nu values increase with Gr_q, but at a slower rate than in the turbulent region downstream.

Unlike stable laminar flows the heat transfer data

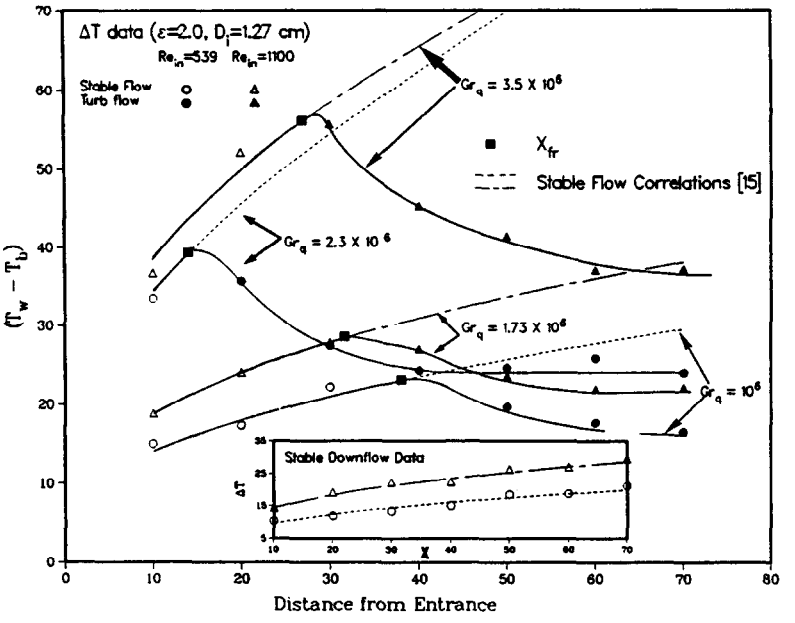

FIG. 10. The measured temperature drop across the boundary layer in buoyancy induced turbulent downflow.

for unstable flows shows no consistent dependence of Nu on axial location. Therefore, the average Nusselt number values, obtained after averaging the local Nusselt numbers over the length of the test section where the flow is stable, were correlated as functions of the heat flux represented by Ra_q and the water mass flux represented by Re_{in}.

Figures 14 and 15 present the developed heat transfer correlations along with the experimental data for buoyancy assisted and opposed flows, respectively. In these figures, the heat transfer correlations were in good agreement with the experimental data: the deviation between the correlations and the data was generally within $\pm 10\%$. As evident from these figures, the heat transfer rates for both buoyancy opposed and assisted flows increase with Ra_q. However, the data exhibited a reverse dependence of Nu on Reynolds number, which may be attributed to the nature of turbulent flow.

Figure 16 compares the heat transfer correlations developed for stable and unstable flows to confirm the continuity of these correlations at the location of flow

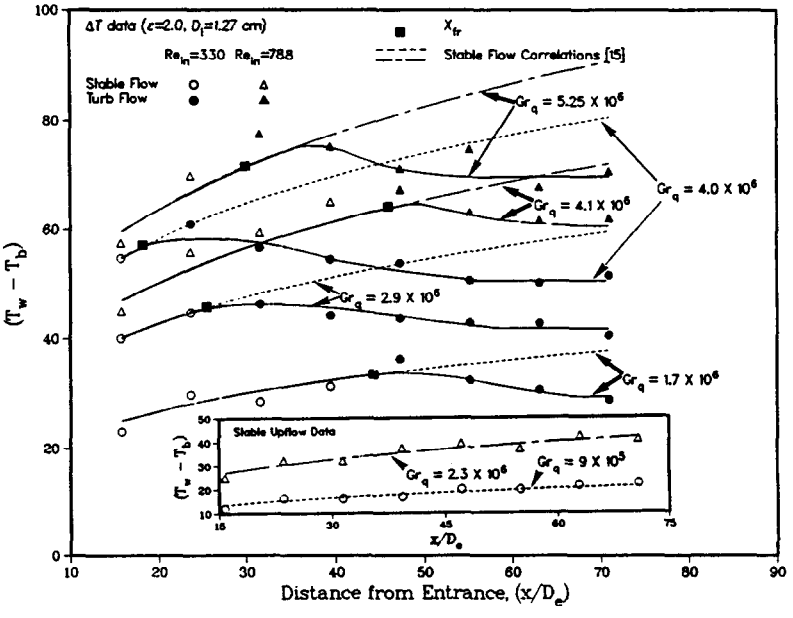

FIG. 11. The measured temperature drop across the boundary laver in buoyancy induced turbulent upflow.

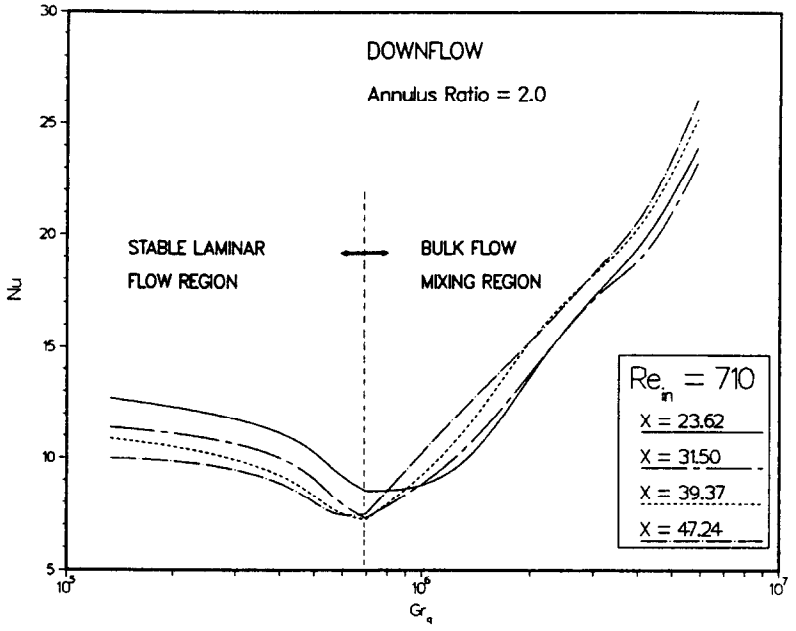

FIG. 12. Effect of the transition to buoyancy induced turbulent downflow on the heat transfer rates.

transition. The stable flow heat transfer correlations were developed in a previous paper by the authors [15]. As evident from Fig. 16, at a given Re_{in} and axial location, X, the Nu values at the corresponding $(Ra_q)_{tr}$ can be predicted either by the stable laminar flow or the turbulent flow correlation; hence confirming the continuity of these correlations at the transition between the two flow regimes. Figure 16 also demonstrates the significant increase in the Nusselt number values in the turbulent flow region compared to those for stable laminar and combined flows at the same inlet Reynolds number.

SUMMARY AND CONCLUSIONS

Flow visualization and heat transfer experiments were performed for low Reynolds number buoyancy assisted and opposed flows in a vertical annulus with uniformly heated inner wall and unheated outer wall. The flow visualization experiments employed two

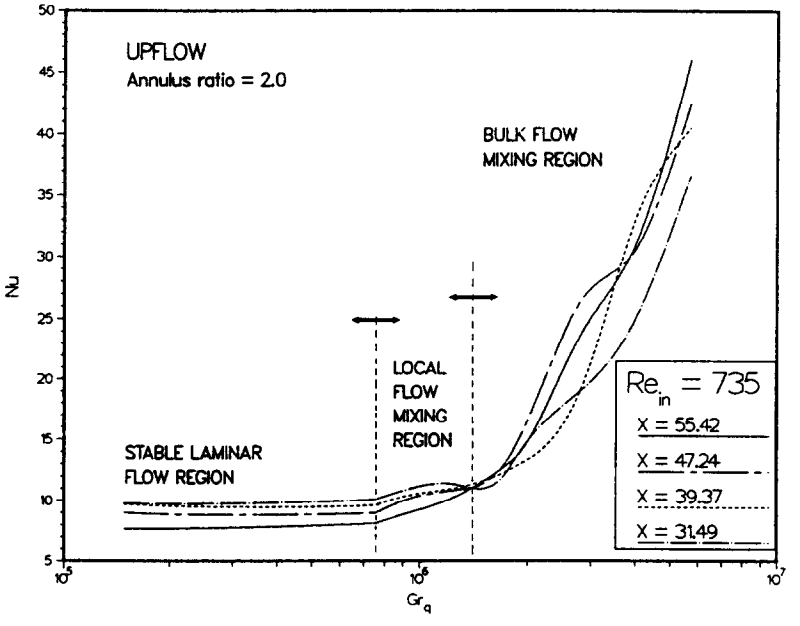

FIG. 13. Effect of the transition to buoyancy induced turbulent upflow on the heat transfer rates.

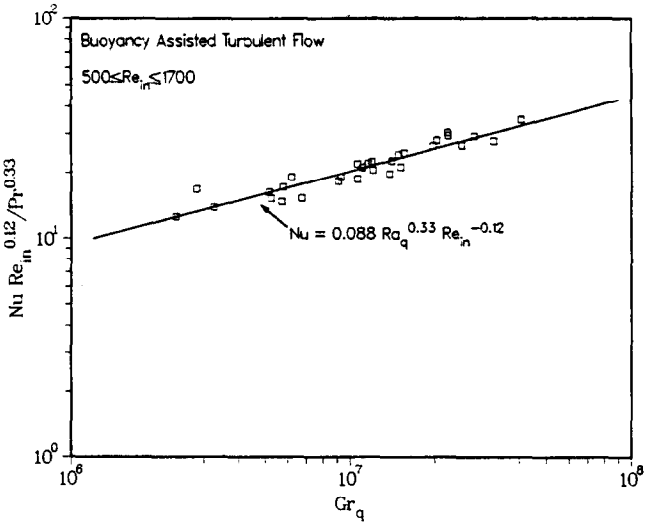

FIG. 14. Heat transfer correlations for buoyancy induced turbulent upflow of water in a vertical annulus having a diameter ratio of 2.

techniques for detecting the onset of flow instability, namely, dye injection and the coolant and wall temperature traces.

The experiments showed that the flow field in the buoyancy assisted flow can be divided into three successive regions: stable laminar flow, local flow mixing, and turbulent regions. In the buoyancy opposed flow, the flow field consisted only of stable laminar flow and turbulent regions. The temperature traces of the heater's surface and coolant temperatures were effective in sensing the onset of flow instability in the experiments. Although the occurrence of the flow instability induced random oscillations downstream, and occasionally upstream, of x_{fr}, the coolant temperatures oscillated only downstream of the location of incipient flow instability. The temperature oscillations in buoyancy opposed turbulent flow were more intense than those recorded for buoyancy opposed flow at the same inlet Reynolds number. Also, the measured differences between the heated wall and water bulk temperatures downstream of x_{fr}, were significantly lower than those for stable laminar flow at the same Re_{in}. Hence it was concluded that the temperature traces technique can be effectively used to detect flow instabilities where visual observation of the flow field is not readily obtainable.

The values of the location of incipient flow instability X_{fr}, which were significantly higher for buoyancy assisted flow than for buoyancy opposed flow, decreased as G_q/Re_{in} was increased; the values of X_{fr} were measured and correlated for both unstable flows. Heat transfer data collected and correlated for

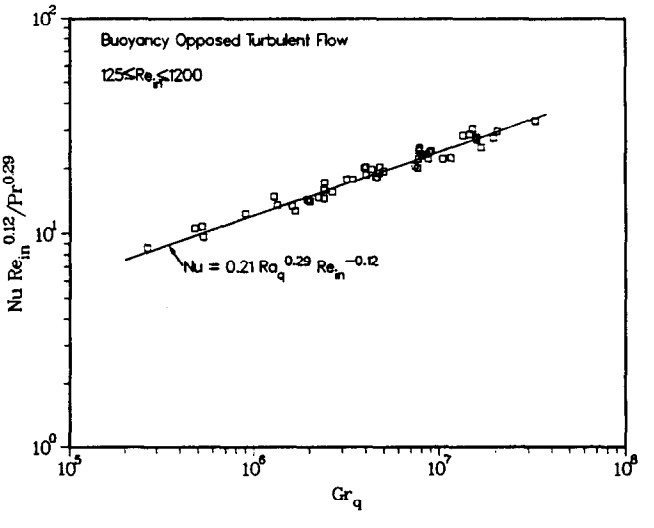

FIG. 15. Heat transfer correlations for buoyancy induced turbulent downflow of water in a vertical annulus having a diameter ratio of 2.

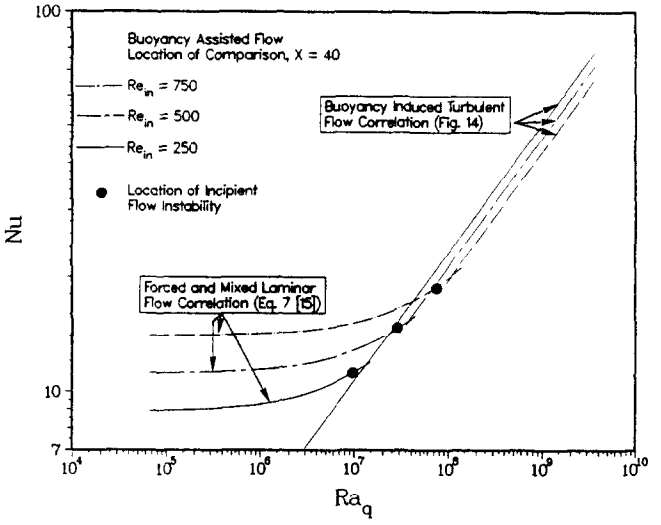

FIG. 16. Comparison of buoyancy induced turbulent flow heat transfer correlations with those for stable combined laminar flow.

unstable flow showed that for Grashof numbers which exceeded threshold values to initiate flow instability, Nusselt number increased rapidly with Grashof number. The measured Nusselt numbers for both buoyancy assisted and opposed turbulent flows were as much as three times higher than those measured for stable laminar flows at the same Re_{in}, but at a lower Gr_q. The values of Nu for both buoyancy assisted and opposed turbulent flows increased as X_{fr} decreased (or turbulent mixing length in the annulus increased). The results of this work could be useful for many applications where buoyancy induced turbulent flow may be encountered. Examples of these applications include waste heat recovery heat exchangers, solar and geothermal energy systems and cooling of nuclear fuel elements in spent fuel storage tanks.

Acknowledgements—The authors gratefully acknowledge the financial support provided by the Sandia National Laboratories and General Atomics Technologies. A special acknowledgement is given to Mr James Schulze of Sandia National Laboratories for his assistance in the design and fabrication of the test section.

REFERENCES

1. B. Gebhart and R. L. Mahajan, Instability and transition in buoyancy-induced flows, *Adv. Appl. Mech.* **22**, 231–315 (1982).
2. K. Sherwin, Combined natural and forced laminar flow in vertical annuli, *Br. Chem. Engng* **14**(9), 1215–1217 (1969).
3. E. M. Rosen and T. J. Hanratty, Use of boundary layer theory to predict the effect of heat transfer of the laminar-flow field in a vertical tube with constant-temperature wall, *A.I.Ch.E. Jl* **7**(1), 112–123 (1961).
4. T. J. Hanratty, E. M. Rosen and R. L. Kabel, Effect of heat transfer on flow field at low Reynolds numbers in vertical tubes, *Ind. Engng Chem.* **50**(5), 815–820 (1958).
5. G. F. Sheele and T. J. Hanratty, Effect of natural convection on stability of flow in vertical pipes, *J. Fluid Mech.* **14**(2), 244–256 (1962).
6. T. M. Hallman, Experimental study of combined forced and free laminar convection in a vertical tube, NASA Technical Report, No. D-104 (1961).
7. G. F. Sheele, E. M. Rosen and T. J. Hanratty, Effect of natural convection on transition to turbulence in vertical pipes, *Can. J. Chem. Engng* **38**, 67–72 (1960).
8. T. E. Mullin and E. R. Gerhard, Heat transfer to water in downward flow in a uniform wall temperature vertical tube at low Graetz numbers, *J. Heat Transfer* **99**, 585–592 (1977).
9. M. A. I. El-Shaarawi and A. Sharan, Free convection effects on the developing laminar flow in vertical concentric annuli, *J. Heat Transfer* **102**, 617–622 (1980).
10. J. H. Kim, Analysis of laminar mixed convection in vertical tube annulus with upward flow. In *Fundamentals of Forced and Mixed Convection* (Edited by F. A. Kulacki and R. D. Boyd), HTD-Vol. 42, pp. 91–98. ASME, New York (1985).
11. D. V. Rao and M. S. El-Genk, Bouyancy induced instability of laminar flows in vertical annuli—II. Model development and analysis, *Int. J. Heat Mass Transfer* **33**, 2161–2172 (1990).
12. B. Metais and E. R. G. Eckert, Forced, free, and mixed convection regimes, *J. Heat Transfer* **86**, 295–296 (1964).
13. E. M. Sparrow, G. M. Chrysler and L. F. Azevado, Observed flow reversal and measured-predicted Nusselt numbers for natural convection in a one-sided heated vertical channel, *J. Heat Transfer* **106**, 325–332 (1984).
14. R. A. Wirtz and P. McKinley, Buoyancy effects on downward laminar convection between parallel plates. In *Fundamentals of Forced and Mixed Convection* (Edited by F. A. Kulacki and R. D. Boyd), HTD-Vol. 42, pp. 105–112. ASME, New York (1985).
15. M. S. El-Genk and D. V. Rao, Heat transfer experiments and correlations for low Reynolds number flows of water in vertical annuli, *Heat Transfer Engng* **10**(2), 44–57 (1989).

INSTABILITE INDUITE PAR FLOTTEMENT POUR DES ECOULEMENTS LAMINAIRES DANS UN ESPACE ANNULAIRE VERTICAL—I. VISUALISATION DE L'ECOULEMENT ET MESURE DE TRANSFERT THERMIQUE

Résumé—Des expériences comprenant à la fois des visualisations et des mesures de transfert thermique ($125 < Re_{in} < 1700$ et $2{,}5 \times 10^5 < Gr_q < 5 \times 10^7$) sont conduites pour étudier l'instabilité, induite par flottement, d'un écoulement laminaire d'eau dans un espace annulaire vertical ayant un rapport de diamètre de 2,0. La paroi interne de l'espace annulaire est uniformément chauffée et la paroi externe est isolée. L'instabilité de l'écoulement est détectée par des images video du champ d'écoulement en dépérissement et la décroissance simultanée de la différence de température entre la paroi chaude et le coeur de l'écoulement d'eau, depuis la valeur laminaire et les fluctuations de la température du liquide. Les valeurs mesurées de x_{fr}, basées sur les images vidéo des champs d'écoulement sont reliées à la fois aux écoulements assistés ou contrariés par le flottement en fonction du nombre de Grashof local, Gr_q, et du nombre de Reynolds local, Re. Les valeurs du nombre de Nusselt pour les écoulements turbulents, induits par frottement en aval de l'apparition de l'instabilité, sont jusqu'à trois fois plus élevées que celles pour les écoulement laminaires stables au même nombre de Reynolds d'entrée, mais pour des Gr_q plus faibles. Le transfert thermique pour les écoulements turbulents induits par flottement est représenté par:

$$Nu = 0{,}088 Ra_q^{0.33}\, Re_{in}^{-0.12} \text{ pour l'ascension}$$

$$Nu = 0{,}21 Ra_q^{0.29}\, Re_{in}^{-0.12} \text{ pour la descente.}$$

AUFTRIEBSINDUZIERTE INSTABILITÄT DER LAMINAREN STRÖMUNG IN EINEM SENKRECHTEN RINGKANAL—I. SICHTBARMACHUNG DER STRÖMUNG UND UNTERSUCHUNG DES WÄRMEÜBERGANGS

Zusammenfassung—Die auftriebsinduzierte Instabilität einer sich entwickelnden laminaren, aufwärts- und abwärtsgerichteten Wasserströmung in einem senkrechten Ringkanal mit dem Durchmesserverhältnis 2 wird durch Strömungsbeobachtung und Wärmeübergangsmessungen untersucht ($125 < Re_{in} < 1700$ und $2{,}5 \times 10^5 < Gr_q < 5 \times 10^7$). Die Innenwand des Ringkanals wird gleichmäßig beheizt, die Außenwand ist wärmegedämmt. Das Einsetzen der Strömungsinstabilität wird aufgrund von Videoaufnahmen des eingefärbten Strömungsfeldes festgestellt, außerdem durch das gleichzeitige Absinken der Temperaturdifferenz zwischen der beheizten Wand und der Kernströmung des Wassers sowie durch Fluktuationen der Kühlmitteltemperatur. Die gemessenen Werte für x_{fr} (aufgrund der Videoaufnahmen) werden für Aufwärts- und Abwärtsströmung in Abhängigkeit von der örtlichen Grashof-Zahl (Gr_q) und der örtlichen Reynolds-Zahl korreliert. Die Nusselt-Zahl in der auftriebsinduzierten turbulenten Strömung hinter dem Ort des Einsetzens der Instabilität ist dreimal so groß wie diejenige für eine stabile laminare Strömung bei derselben Eintritts-Reynolds-Zahl und geringerer Grashof-Zahl. Für den Wärmeübergang bei auftriebsinduzierter turbulenter Strömung werden folgende Gleichungen angegeben:

$$Nu = 0{,}088 Ra_q^{0.33}\, Re_{in}^{-0.12}, \text{ für Aufwärtsströmung}$$

$$Nu = 0{,}21 Ra_q^{0.29}\, Re_{in}^{-0.12}, \text{ für Abwärtsströmung.}$$

НЕУСТОЙЧИВОСТЬ ЛАМИНАРНЫХ ТЕЧЕНИЙ В ВЕРТИКАЛЬНЫХ КОЛЬЦЕВЫХ КАНАЛАХ, ВЫЗВАННАЯ ПОДЪЕМНЫМИ СИЛАМИ—I. ЭКСПЕРИМЕНТЫ ПО ВИЗУЛИЗАЦИИ ТЕЧЕНИЯ И ТЕПЛОПЕРЕНОСУ

Аннотация—Проведены эксперименты, включающие визуализацию течения и измерения теплопереноса, для исследования влияния подъемных сил на устойчивость восходящего и нисходящего течений воды в вертикальном кольцевом канале с отношением диаметров 2,0. Внутренняя стенка канала равномерно нагрета, внешняя—изолирована. Начало неустойчивости обнаруживается по изображениям окрашенного поля течения, одновременному уменьшению разности температур между нагретой стенкой и объемом воды по сравнению с ламинарным значением, а также по колебаниям температуры хладагента. Значения x_{fr}, полученные на основе визульных изображений окрашенных полей течения, коррелируются для течений как с совпадающим, так и противоположным действием подъемных сил и вынужденного потока в зависимости от локальных значений чисел Грасгофа Gr_q и Рейнольдса Re. Значения числа Нуссельта для вызванных подъемными силами турбулентных течений, определяемые ниже по течению от места возникновения неустойчивости, в три раза выше, чем для устойчивых ламинарных течений при одинаковом значении числа Рейнольдса на входе, но более низком значении Gr_q. Установлены следующие зависимости для результатов теплопереноса при обусловленных подъемными силами турбулентных течениях:

$$Nu = 0{,}088 Ra_q^{0.33}\, Re_{in}^{-0.12} \quad \text{для восходящего течения}$$

$$Nu = 0{,}21 Ra_q^{0.29}\, Re_{in}^{-0.12} \quad \text{для нисходящего течения.}$$